www.cad-journal.net
Computer-Aided Design AND APPLICATIONS™

Influence of Spool Bore Position on the Structural and Hydraulic Performance of an Additively Manufactured NG10 Valve

Jan Bartolj[1], Aljaž Žafran[1], Nikola Vukašinović[1] and Franc Majdič[1]

[1]University of Ljubljana, Faculty of mechanical engineering, Aškerčeva cesta 6, 1000 Ljubljana, Slovenia; https://www.fs.uni-lj.si/

Corresponding author: Franc Majdič, franc.majdic@fs.uni-lj.si

Abstract. This study investigates the influence of spool bore position on the hydraulic and structural performance of an additively manufactured NG10 hydraulic valve. A workflow combining parametric CAD modelling, computational fluid dynamics, and topology optimization was applied to evaluate different vertical and lateral spool bore offsets. For each configuration, pressure drop, turbulent kinetic energy dissipation and final optimized mass were assessed, followed by a trade-off analysis. The results showed that the optimal configurations for mass, pressure drop, and turbulent kinetic energy dissipation reduction do not coincide, confirming the conflicting nature of the design objectives. This indicates that spool bore position should be treated as an active design variable when seeking improved valve performance. The proposed workflow supports early decision-making for lightweight and hydraulically efficient additively manufactured valve components, depending on the prioritized performance criteria.

Keywords: Topology optimization, Flow analysis, Hydraulic valve, Additive manufacturing
DOI: https://doi.org/10.14733/cadaps.2027.68-86

1 INTRODUCTION

Industrial applications are experiencing ever-rising demands for high-performance components and systems [28]. Especially in cases where motion or dynamic behaviour is required, hydraulics is usually the preferred solution. This is due to the simplicity and accessibility of the components, combined with impressive and almost unmatched power density. When considering hydraulic components, most of them generate pressure losses as a side effect because the flow is internally restricted. To reduce these internal losses, which typically only result in excess heat generation, some form of optimization is required. The largest contributors to pressure drop in hydraulic systems are valves, which direct and regulate the flow of fluid.

Hydraulic valves are typically manufactured with relatively simple internal geometries due to traditional machining constraints. Sub-optimal internal geometries are usually the primary cause of pressure losses, consequently increasing fluid temperature and reducing both efficiency and service life. Optimization of both the internal geometry of flow channels and material distribution is possible when designing for AM [1-4, 9, 17, 23, 26, 27]. AM enables the realization of highly complex internal flow paths compared to conventional production technologies, thereby improving hydraulic performance.

As mentioned, AM also enables the optimization of external geometry. External geometry is typically optimized to conserve material and reduce the mass of the component using topology optimization (TO). Many studies have focused on the optimization of external geometries, achieving significant material savings and consequently reducing the mass of the final part [6, 10-12, 18, 20, 22, 24, 29]. However, these approaches usually assume a fixed internal structure. Valve inlet and outlet connections are typically positioned according to standards and cannot be modified, whereas the internal geometry of the flow channels and the position of the spool bore remain adjustable. Recent studies indicate that TO can yield improved solutions when variables that are typically fixed during preprocessing are incorporated into the optimization framework and allowed to vary. Maruyama et al. [19] treated these variables as parameters defining the design domain boundary conditions and demonstrated that optimizing them together with material distribution can enhance the final result. Lee and Xie [16] similarly showed that the number, position, and stiffness of supports can significantly influence the optimal topology, while Zheng et al. [30] demonstrated that, for design dependent pressure loading, the position and direction of the load evolve together with the topology itself. More recently, Rong et al. [21] proposed an adaptive support design approach in which the support layout is optimized during the optimization process.

Research group from ETH Zurich has been researching the field of hydraulics and AM, mainly developing design methodologies and software-supported workflows. Their work is mainly focused on Computational Fluid Dynmacis (CFD) driven internal channel optimization and automated geometry generation taking AM constraints into consideration [7, 13]. Their research group did make a brief study on optimization of internal structure of the hydraulic valve [14], but the result has a very limited industrial applicability because of the extremely unconventional spool bore placement.

A research gap was identified in the variable positioning of the spool bore within hydraulic valves and its effect on performance and efficiency, from both structural and hydraulic perspectives. To address this, a size 10 hydraulic valve (CETOP 5) was selected due to its complex internal structure and widespread industrial use. Material distributions of valves with different spool bore positions were optimized using TO to evaluate the impact on mass and structural performance. All configurations were additionally analyzed in terms of their flow characteristics.

Figure 1: 3D printed hydraulic valve (size 3 according to CETOP), designed using TO and extensive CFD testing.

The central research question is how to define a workflow that captures the influence of key geometric design variables, such as spool bore position, on both hydraulic and structural performance. Main contributions of this study are:

- Establishing a workflow for the design of hydraulic components for AM on a real industrial case
- Parametric study of spool bore position
- Identification of trade-offs between mass reduction and flow characteristics based on spool bore position

2 METHODOLOGY OVERVIEW

TO has proven to be a highly effective tool for determining optimal shapes [1, 17, 20] and, consequently, material consumption. Such optimal shapes are often characterized by complex geometries that are difficult to manufacture and therefore require alternative processes such as AM. AM, in combination with TO, has been applied in multiple studies to improve specific characteristics of hydraulic components, with a particular focus on enhancing flow dynamics.

The first step toward improving hydraulic parameters, and consequently overall efficiency, is the optimization of the internal structure of individual components. The hydraulic performance associated with a given geometry can be evaluated numerically using CFD software. However, there is no standardized approach for optimization, simulation, and the overall development cycle of AM hydraulic valves. As a result, engineers typically rely on prior experience and established best practices.

The proposed methodology is formulated as a modular workflow that uses numerical flow simulation and structural TO which are linked by common geometric parameters. The workflow is designed to enable consistent evaluation of interacting design variables and can be applied to a broad class of hydraulic components manufactured using AM technologies.

For this study, a size 10 hydraulic valve, according to ISO 4401 [15] and equivalent to CETOP 5 [8], was selected. This valve was used as a reference model, with the main limitation being the constraints imposed by conventional manufacturing methods. The valve can be produced using simple milling operations; however, this results in an internal geometry characterized by sharp edges and abrupt changes in cross-section, which lead to increased turbulence and hydraulic losses. The CAD geometry of the valve body is presented in Figure 2 (right), while the standardized holes and bottom plate design are shown in Figure 2 (left). As a basis for this study, a workflow was defined, as presented in Figure 3. In the first step, the inlet and outlet port positions defined by ISO 4401 were adopted. Then, parametric CAD models are created based on selected configurations for evaluation. For each configuration a model is created for CFD analysis and for TO. The results are then evaluated and trade-offs for pressure drop, TKE dissipation and final mass are identified based on spool bore position. In the final step, selected configuration would then be prepared for manufacturing, however, this step is out of scope of this work.

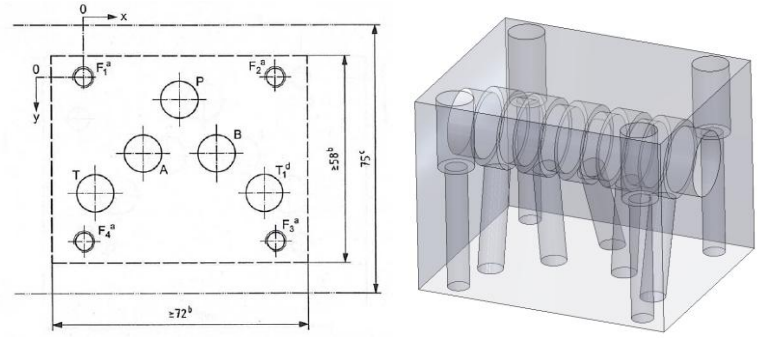

Figure 2: Standard configuration of the bottom side of the hydraulic valve according to ISO 4401 size 10, and CAD model of a conventionally manufacturable hydraulic valve of the same size.

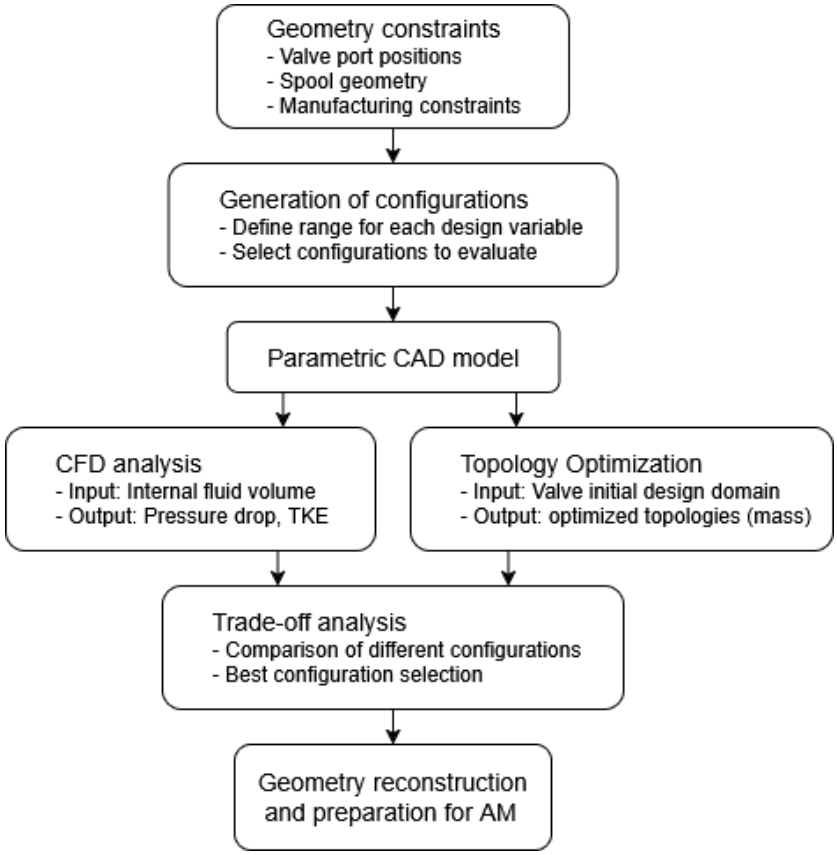

Figure 3: Proposed workflow for valve design.

The described workflow establishes a consistent link between design variables, numerical evaluation, and structural optimization. By combining CFD and TO within a shared parametric framework, it enables the identification of interacting trends between hydraulic performance and structural response. The following results demonstrate the applicability of this workflow and its ability to support multi-objective design decisions. Subsequently, the lowest height from the bottom plane at which the spool bore can be positioned was defined. Based on the known spool geometry, internal toroidal voids were parametrically generated, taking AM restrictions into account. Finally, a loft-cut feature was used to connect the standardized bottom holes with their corresponding toroidal voids around the spool. In this manner, a fully parametric model of the internal structure was created, enclosed within an outer box-shaped, unoptimized domain. To complete the valve model, a separately designed spool for proportional valves was assembled into the final geometry.

Since the goal of this study was to evaluate the position of the spool bore with respect to the overall structure, a design matrix of different spool configurations was established. As the magnetic coils controlling the spool opening inside the valve body have a radius of 37 mm, the minimum spool vertical offset was defined as 40 mm. To determine the optimal spool bore position, five lateral positions from -10 to 10 mm were considered in increments of 5 mm. Figure 4 illustrates the position of the spool bore for a spools with vertical offset of 40 mm and a lateral offset of 5 mm.

Besides the five lateral bore positions, three vertical offset levels were defined in increments of 10 mm, with 40 mm as the minimum and 60 mm as the maximum. At this stage, it was expected that the lowest spool vertical offset would result in the highest resistance to flow through the valve, while being the most favourable for TO.

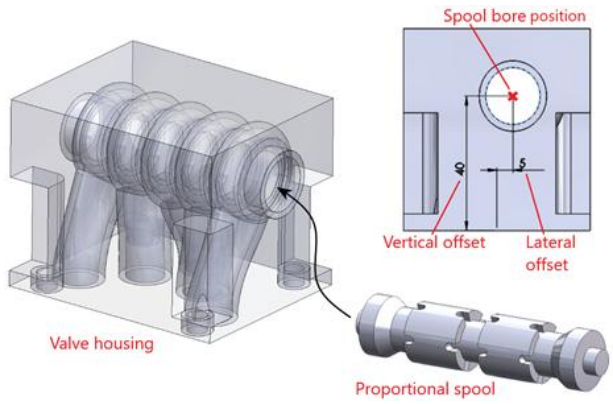

Figure 4: CAD model of valve housing block with optimized internal geometry for better flow efficiency and proportional spool.

For higher spool vertical offsets, the mass was expected to increase due to the additional material required to satisfy structural stiffness. However, this may be beneficial in terms of pressure losses, as fewer abrupt geometric changes are encountered by the fluid flowing through the valve body. The different spool bore positions are illustrated in Figure 5.

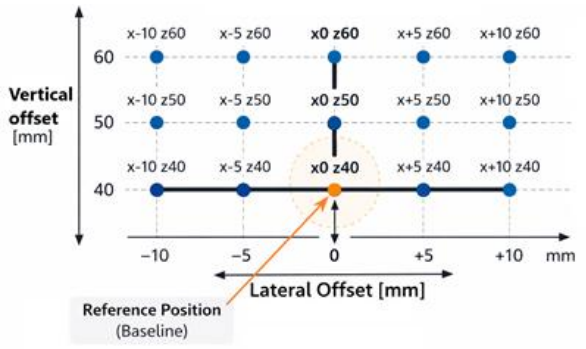

Figure 5: Parametric design cases that explain 15 different spool bore positions.

When the internal structures, together with the spool bore and its positional variations, were defined, they were extracted as a basis for CFD simulations. Since fluid flow behaviour was one of the criteria for determining the optimal configuration, four different flow rates were considered in increments of 20 L/min. As the nominal flow rate of size 10 valves is 120 L/min, the simulations covered a range from 60 to 120 L/min.

After the CFD simulations were completed, the outer geometry of the valves was analysed. TO was performed to identify lightweight material distributions that satisfy the required structural performance under realistic operating loads. Structurally efficient concepts were generated for each spool bore position variant and evaluated based on the mass of the resulting topology.

In the subsequent steps, the results from both analyses were evaluated and compared to identify the most suitable candidate, considering both TO and CFD results. The results are presented within the context of the proposed workflow, with the aim of assessing how effectively it captures the interaction between spool bore position and both hydraulic and structural performance. Rather than focusing on a single optimal design, the analysis emphasizes trends and trade-offs that emerge from the systematic variation of design parameters.

3 HYDRAULICS, VALVES, AND CFD

In hydraulics, energy losses originate from different sources, mostly linked to pressure drops, and can be divided into two categories: hydraulic friction losses and local losses. Hydraulic friction losses are defined by the shape and condition of pipes or other types of manifolds. Local losses, on the other hand, arise from sudden changes in the geometry through which the fluid flows. Sharp and rough geometries introduce so-called "dead volumes" and potential regions of recirculation where turbulence may occur. Local losses typically account for a larger share of total losses compared to linear losses within hydraulic manifolds and valves. Within a hydraulic valve, both the magnitude and direction of the flow are influenced by spool movement, making this a crucial aspect of the overall geometry. In this study, a proportional spool was used, where specially designed notches regulate the flow rate by restricting the effective flow cross-section. As the spool opening directly influences the internal topology of the valve, and this parameter was not included as a variable, it was fixed at 3 mm, corresponding to 75% opening. Since notch geometry on the spool greatly reduces cross-sectional area and introduces localized losses compared to conventional spools, somewhat higher-pressure losses are expected. But main advantage of proportional hydraulic valves is ability to precisely control the amount of the flow besides general direction.

For the CFD simulations, ANSYS Fluent 2025 R1 software was used. Fluid flow was modelled as single-phase, Newtonian, steady-state, and incompressible. In all simulations, liquid water was used with standard properties: density of 998.2 kg/m³ and dynamic viscosity of $10.03 \cdot 10^{-4}$ kg/m·s. Water was used as the working fluid due to its lower viscosity, which promotes turbulence development, while also aligning with current research efforts toward environmentally acceptable hydraulic fluids.

Turbulence was modelled using the k–ε model. k–ε turbulence model is numerically stable and less sensitive to mesh quality. Since CFD simulations were not the primary focus of this study and objective was mainly to study trends and relative differences in pressure drop and velocity fields authors have chosen this robust and consistent turbulent model to achieve efficient repeatability and usage of hardware resources during parametric studies. The governing equations include conservation of mass, defined by equation (1):

$$\nabla \cdot \mathbf{u} = 0 \tag{1}$$

and conservation of momentum (2):

$$\rho(\mathbf{u} \cdot \nabla)\mathbf{u} = -\nabla p + \nabla \cdot \bar{\boldsymbol{\tau}} + \mathbf{F} \tag{2}$$

where **u** is the velocity vector, **p** is the pressure, **ρ** is the density, $\bar{\boldsymbol{\tau}}$ is the Newtonian viscous stress tensor, and **F** represents additional body forces. Pressure–velocity coupling was handled using the SIMPLE algorithm. Boundary conditions were defined as velocity inlets and pressure outlets, with no-slip conditions applied to all walls. The meshes were unstructured, with refined boundary layers. Velocity inlet conditions were calculated based on the flow rates 60, 80, 100, and 120 L/min. The spools transversal displacement, which primarily restricts the flow, was set to 3 mm, as shown in Figure 6. Figure 6 (left) presents the conventionally manufactured valve with a simple internal geometry, while Figure 6 (right) shows the more complex and optimized internal structure designed for AM.

Red arrows originating from the bottom plane represent the inlet into the pressure chamber of both valves and correspond to the velocity inlet boundary condition. When the spool is transversely shifted to one side, the geometry is divided into two separate flow paths. The first path, entering the valve through the pressure port, is connected to working line A and is represented by blue arrows in Figure 6. The second path is connected to working line B, represented by orange arrows, and leads to the relief line, which is typically connected to the hydraulic reservoir at ambient pressure, indicated by the green arrow.

Extracted internal volumes prepared for CFD simulations are shown in Figure 7. The separated flow domains can be clearly observed. Pressure drops are evaluated for each volume individually, defined as the difference between inlet and outlet pressures.

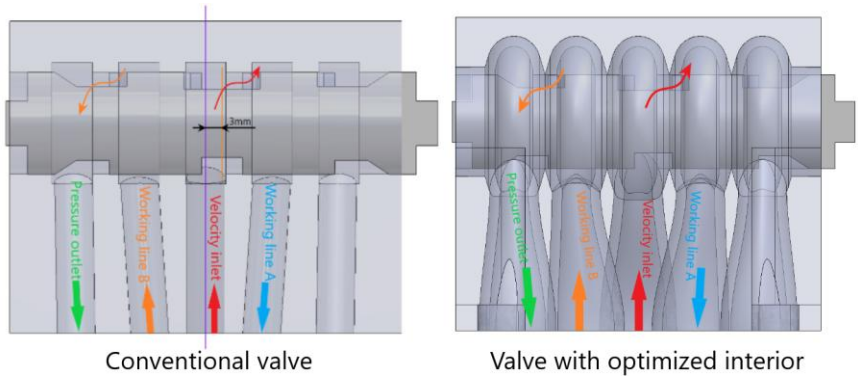

Figure 6: CAD of reference conventionally manufacturable hydraulic valve body and CAD of optimized AM hydraulic valve body with spool.

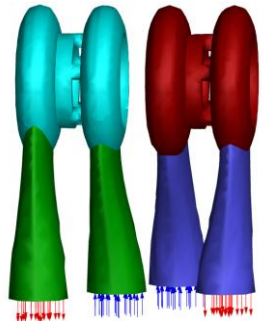

Figure 7: Extracted fluid volumes, base for CFD simulation and evaluation of hydraulic parameters.

For meshing, the ANSYS Fluent Meshing module was used. Local refinements were applied to capture flow features in critical regions as shown in the Figure 8. In particular, the mesh density was increased near the spool using local sizing zones to resolve velocity gradients and potential flow separation. For improved near-wall behaviour, five boundary layers were applied to solid surfaces. This meshing strategy provides a balance between computational efficiency and accurate resolution of relevant flow phenomena.

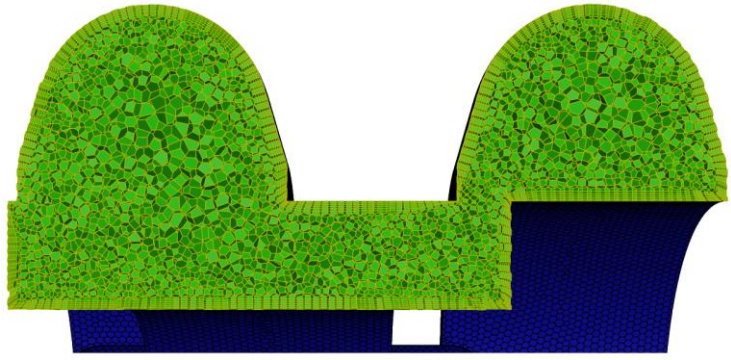

Figure 8: Example of mesh section on the critical part of the geometry.

To verify that the applied mesh resolution is sufficient to capture the relevant flow features, a mesh independence study was conducted shown on the Figure 9. The results show rapid convergence of inlet pressure with increasing mesh density. Significant deviations are observed for coarse meshes, while the solution stabilizes for meshes exceeding approximately 1 million elements. The relative difference between successive refinements falls below 2.5%, indicating reliable and consistent results. Therefore, a mesh with approximately 1.2 million elements was selected as a compromise between accuracy and computational cost.

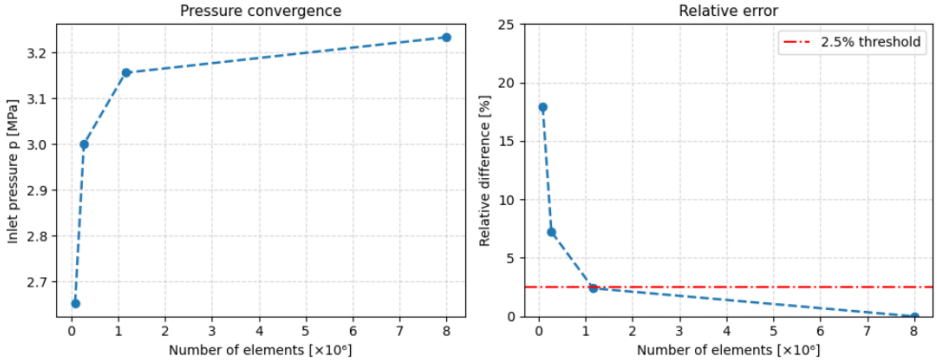

Figure 9: Mesh independence study for CFD.

The performance of each design was evaluated based on several criteria. The main indicator of flow conditions inside the valve was the pressure drop. As mentioned previously, the pressure drop was calculated between inlet and outlet ports using equation (3), where Δp represents the pressure drop through the valve, and $p_{inlet}$and p_{outlet}represent the calculated pressures at the respective ports.

$$\Delta p = p_{inlet} - p_{outlet} \tag{3}$$

The second performance metric used to evaluate the internal valve design based on fluid flow was the velocity field. Flow uniformity or non-uniformity was used as an indicator to assess "flowability," considering continuity, the presence of "dead volumes," and recirculation regions, which contribute to turbulence and hydraulic losses.

Lastly, turbulence was evaluated based on the calculated results. The magnitude and distribution of turbulence detected in critical regions can have a significant impact on determining whether a design is suitable for further evaluation.

Typical time for each calculation to reach convergence criteria was around 45 minutes. This was done at previously explained and presented boundary conditions.

4 TOPOLOGY OPTIMIZATION

In structural topology optimization, the problem is commonly formulated as the minimization of compliance, subject to a constraint on the allowable material volume. In this standard form, the aim is to determine the most efficient material distribution within a prescribed design domain for given loads, boundary conditions and constraints [5, 25]. In the present work, however, the optimization problem was adapted to better reflect the requirements of the investigated hydraulic valve. Instead of considering only compliance with a volume constraint, the objective function was defined as a weighted combination of compliance and mass in order to minimize mass while keeping structural integrity. Displacement constraint was imposed in the spool-guiding region to ensure that the maximum allowable radial deformation was not exceeded. For our problem, formulation (4) is

$$\begin{aligned} &min: && J(\rho) = w_1\,\hat{C}(\rho) + w_2\,\hat{M}(\rho), && (4)\\ &subject\ to: && K(\rho)\,u\,(\rho) = F, \\ & && u_{spool,r,max}(\rho) \le u_{allow}, \\ & && 0 \le \rho_e \le 1, \qquad e = 1,\dots,n, \end{aligned}$$

where $J(\rho)$ is the objective function, $\hat{C}(\rho)$ and $\hat{M}(\rho)$ denote compliance and mass normalized by their initial values respectively, and w_1 and w_2 are the corresponding weighting factors. The unnormalized compliance (5) is evaluated as

$$C(\rho) = F^T u(\rho). \qquad (5)$$

$K(\rho)$, $u(\rho)$, and F denote the global stiffness matrix, displacement vector, and load vector, respectively. The constraint $u_{spool,r,max}(\rho) \le u_{allow}$ limits the maximum radial displacement in the spool-guiding region to the allowable value.

The valve body was assumed to be manufactured from MS1 maraging steel, a material commonly used in AM due to its high strength. Density of 8100 kg/m³, Young's modulus of 180 GPa, Poisson's ratio of 0.3 and yield strength 2010 MPa was used. The applied loading and boundary conditions were defined to represent mechanical actions acting on the valve body during service. A maximum internal pressure of 350 bar was applied to the internal channel walls. In addition, axial forces of 5000 N were imposed on both end faces of the spool bore, while counteracting forces of the same magnitude were applied to the inner surface of the spool bore. To represent screw loading, an additional force of 3000 N was applied to the regions around the fastening holes. The valve body was constrained by cylindrical supports at the fastening holes, with radial displacement restricted, while the lower surfaces around these holes were fixed in the normal direction.

The topology optimization was performed in Ansys Mechanical and with density-based Solid Isotropic Material with Penalization (SIMP) method with a penalization factor of 3 and initial volume fraction of 0.5. To preserve functionality, several regions were excluded from the optimization domain. These excluded regions were the spool contact surfaces, mounting and fastening surfaces, port related surfaces and all areas used for load and support definition. Since the spool guidance region is particularly important for correct valve function, displacement constraint was imposed by limiting the radial displacement of the inner spool contact walls to less than 0.01 mm (Figure 10). This ensured that the achieved mass reduction did not compromise the stability required for proper spool motion. To improve the manufacturability of the optimized designs, additional topology optimization constraints were introduced. First, the minimum member size was set to 2 mm in order to prevent the formation of excessively thin structural features that would be difficult to manufacture. Second, an additive manufacturing overhang constraint of 45° was applied. This was used to reduce the occurrence of unsupported material and thereby limit the need for support structures during fabrication.

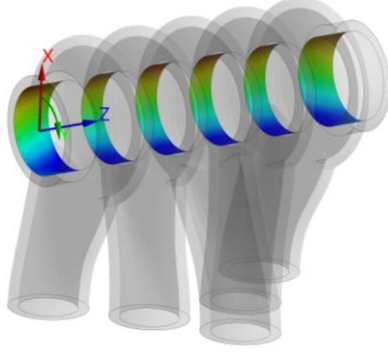

Figure 10: Example of inner spool contact surfaces that are under deformation constraint.

Topology optimization was carried out in Ansys Mechanical using the complete valve block as the initial design domain. The optimization model was discretized with tetrahedral elements. To ensure that the selected mesh provided a suitable balance between numerical accuracy and computational cost, a mesh convergence study was first performed on the configuration $Z = 40$ mm, $x = 0$ mm with a weight ratio of 1:1 for compliance and mass objectives. Element sizes of 2 mm, 1 mm, 0.67 mm and 0.5 mm were tested. In Figure 11, it can be observed that the convergence plot does not look much like usual FEA convergence plots. This is mainly due to the interaction between minimal member size and element size. The minimum member size is linked to the mesh resolution and should be represented by several finite elements across the smallest admissible feature. Slight variation of results can happen due to the dependence of TO results on generated mesh which may cause the solver to find slightly different local optima or result in different stopping behaviour. The 0.5 mm mesh yielded very similar result to the 0.67 mm mesh with a difference of 0.6 %, while requiring higher computational effort. Also, the material distributions of the designs were very similar. The 0.67 mm element size was therefore selected for the study. With a target minimum member size of 2 mm, this provided approximately three elements across the smallest structural member, which was considered sufficient for reliable representation of the optimized geometry.

The objective function was defined as a weighted combination of compliance minimization and mass minimization. In the TO part of this study, the main emphasis was on mass removal, which is why several weighting ratios in the range from 1:1 to 1:10 in favour of mass minimization were evaluated using the same representative configuration as in the mesh convergence study. As shown in Figure 12, lower weighting ratios produced more conservative topologies with less removed material and faster convergence. Increasing the relative weight of mass minimization led to progressively lower retained mass, but also increased the required computational effort. Although ratios higher than 1:5 resulted in additional mass reduction, the weighting factor selection was treated as a design choice for defining a consistent TO setup, rather than the primary optimization objective of this study. The main aim was to compare the influence of spool bore position under identical optimization settings. Since the optimized topology serves as a basis for subsequent geometry reconstruction rather than as a directly manufactured geometry, the selected ratio was considered sufficient for defining a consistent comparative TO setup. Therefore, the 1:5 ratio was selected as a practical compromise, providing substantial material removal while maintaining acceptable computational efficiency and stable convergence. The same weighting ratio was then applied to all spool bore configurations to ensure comparability between cases.

5 RESULTS AND DISCUSSION

5.1 Flow Analysis

Compared to the conventional design, optimized internal geometries exhibit a more uniform velocity distribution and reduced high-velocity regions in critical areas. In particular, the configuration with a spool vertical offset of $Z = 60$ mm and a lateral offset of $x = 0$ mm shows a smoother flow transition through the valve, with reduced recirculation and lower peak velocities, resulting in the lowest pressure drop of 14.95 MPa (≈149.5 bar) at 120 L/min. Such elevated pressure losses are expected due to the significant flow restriction introduced by the proportional spool configuration. In contrast, the conventional design exhibits localized acceleration and a less uniform flow distribution, which contributes to higher pressure losses, calculated to be 21.36 MPa (≈213.6 bar). This represents an improvement of approximately 30 % for the optimized design. These observations are consistent with the quantitative results presented in Figure 13 which represents 3 different geometries of pressure channel at a spools bore vertical offset of $Z = 40$ mm.

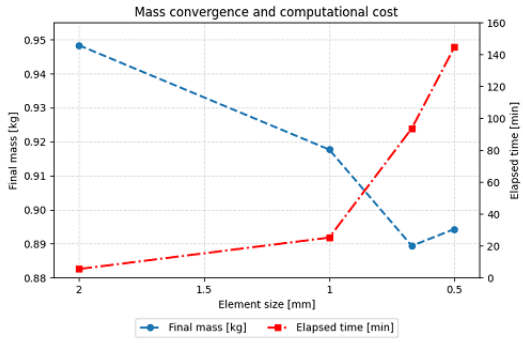

Figure 11: Mass convergence analysis and computational cost depending on element size.

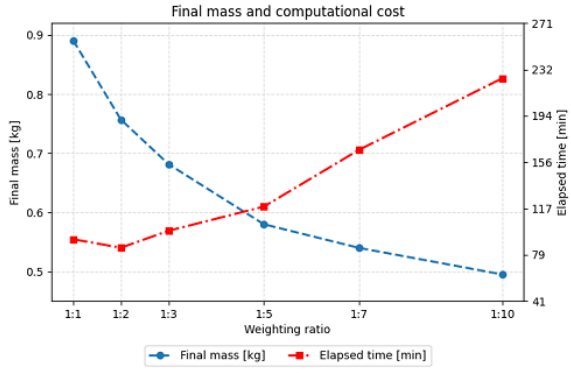

Figure 12: Final mass and computational cost for different weighting ratios.

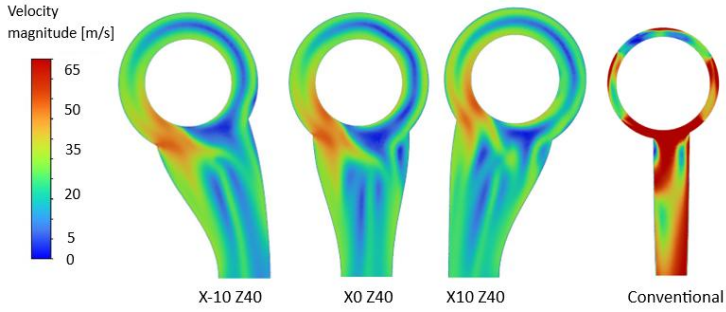

Figure 13: Cross-section of a hydraulic channel, with different lateral bore positions explained and CFD results of velocity contours. Compared to cross-section of velocity contours from conventionally manufacturable hydraulic valve.

The pressure drop distribution as a function of lateral offset and spool bore vertical offset is presented in Figure 14. The discrete CFD evaluation points are indicated by markers, while the continuous field is obtained via cubic interpolation to facilitate trend identification. A clear non-monotonic dependence on lateral bore offset can be observed. For all investigated spool bore vertical offsets, the pressure drop decreases when moving from extreme negative offsets toward a central or slightly positive bore

position, followed by an increase toward extreme positive bore offsets. While the minimum pressure drop is achieved at a local minimum around $x = 0$ mm and $Z = 60$ mm, with a value of $\Delta p = 14.95$ MPa (≈150 bar) at 120 L/min, the best averaged results are observed at a spool bore vertical offset of $Z = 40$ mm within lateral offsets of ±5 mm. In contrast, the highest pressure drop is observed at $x = 10$ mm and a spool bore vertical offset of $Z = 50$ mm, reaching $\Delta p = 15.71$ MPa, indicating a strong sensitivity of the flow to lateral misalignment. The difference between the best and worst configurations amounts to approximately 5 %, highlighting the significance of spool bore lateral offsets as a design parameter. The influence of spool bore vertical offset is less pronounced than that of lateral bore offset but remains noticeable. Compared to the conventional design ($\Delta p = 21.36$ MPa ≈ 214 bar), the optimal configuration achieves a reduction of approximately 30 %, demonstrating the potential of geometric modification for improving hydraulic performance. Compared to the baseline configuration $Z = 40$ mm and $x = 0$, the best configuration achieved a 1.8 % reduction in pressure drop.

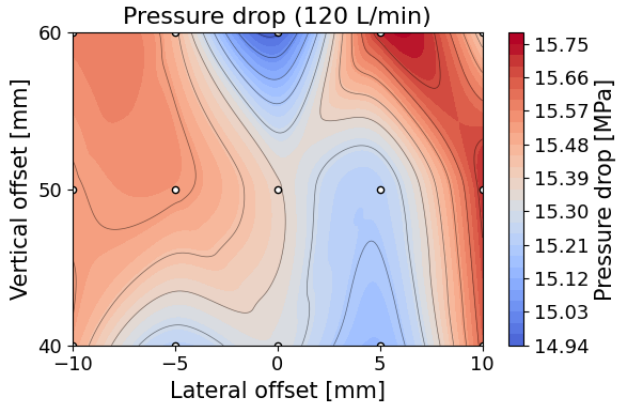

Figure 14: Calculated colourmap results of pressure drop obtained from CFD numerical simulations for different lateral and vertical offsets of spool bore.

The distribution of turbulent kinetic energy (TKE) dissipation as a function of lateral offset and spool bore vertical offset is shown in Figure 15. The discrete CFD evaluation points are indicated by markers, while the continuous field is obtained via cubic interpolation to highlight general trends within the design space. In contrast to the pressure drop behaviour, TKE dissipation exhibits a more pronounced sensitivity to both lateral offset and spool bore vertical offset. Lower dissipation levels are predominantly observed in the region of $x = 5$ mm, particularly for $Z = 40$ mm, where values reach approximately 95.3 m²/s², indicating smoother and less energy-dissipative flow. Conversely, significantly higher dissipation levels occur at extreme positive lateral offsets (e.g., $x = 10$ mm), where TKE values increase to approximately 180 m²/s², suggesting intensified turbulence and higher energy losses due to flow separation and local acceleration effects. The difference between minimum and maximum dissipation exceeds 50 %, highlighting the strong influence of geometric configuration on flow structure. Importantly, the regions of minimum TKE dissipation do not fully coincide with the locations of minimum pressure drop identified in Figure 14. This indicates that configurations optimizing pressure losses do not necessarily minimize turbulence-related losses, confirming the multi-objective nature of the design problem. Compared to the baseline configuration, the best configuration achieved a 17.4 % improvement.

Representative distributions of TKE dissipation for selected configurations are shown in Figure 16. The optimized geometries exhibit a more uniform dissipation field with reduced localized peaks compared to the conventional design, where regions of high dissipation are concentrated near sharp geometric transitions.

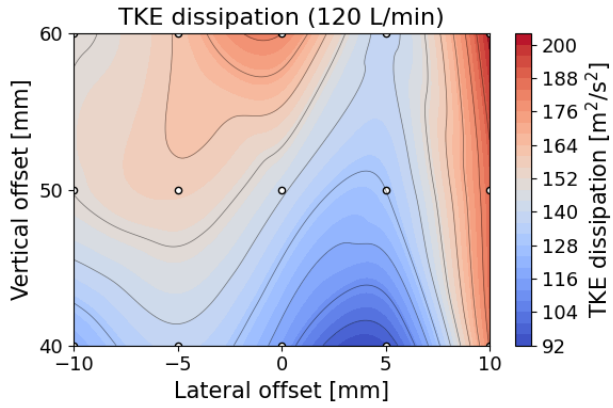

Figure 15: Calculated colourmap results of TKE dissipation obtained from CFD numerical simulations for different lateral and vertical offsets of spool bore.

These results support the quantitative trends observed in Figure 15, indicating that appropriate adjustment of spool bore lateral offset can reduce turbulence intensity and promote smoother flow development. On the Figure 16, it can be observed how do conventional and AM designs compare. Since conventional design is limited to conventional tools path logically cross-sections are smaller and unoptimized. Consequently, amount of turbulence expected and calculated is much higher.

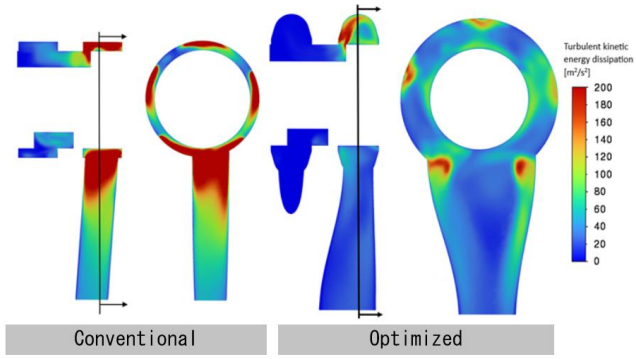

Figure 16: Comparison of lateral and transversal cross-section velocity profiles for Conventional and optimized AM hydraulic valve body.

The CFD analysis demonstrates that spool bore vertical and lateral offset has a measurable influence on hydraulic performance, with lateral offset identified as the dominant parameter. The optimal configuration is difficult to define, as this represents a multi-objective problem with multiple viable solutions. However, since the minimum pressure drop of $\Delta p = 14.95$ MPa (≈150 bar) is located at $x = 0$ mm and $Z = 60$ mm, and the lowest TKE dissipation is observed at $x = 5$ mm and $Z = 40$ mm, a suitable compromise configuration can be identified around $x = 5$ mm and $Z = 50$ mm. This point exhibits relatively low values across both evaluation metrics, although it does not represent a global minimum. Compared to the respective optimal values, this configuration results in only a 2% increase in pressure drop and a 23% increase in turbulence. As the locations of minimum pressure drop and minimum TKE dissipation do not fully coincide, it can be concluded that hydraulic behaviour is governed by competing effects.

5.2 Topology Optimization

Initial masses of the valve blocks prior to TO ranged from 1.47 kg to 2.07 kg. Overall, optimized designs achieved a mass reduction of around 60% compared to the initial solid blocks before the optimization. Effects of spool bore position on material layout for some of the configurations can be seen in Figure 17. Material is mainly retained near functional regions and along load paths, showing that the optimized topology depends on the spool bore position. The results indicate that the spool bore vertical offset has a much stronger influence on mass than the lateral offset. Variation in final mass is of approximately 0.2 kg when looking at vertical offset, while lateral offsets provide smaller variation in results of up to approximately 0.05 kg. As expected, the lowest masses were obtained at $Z = 40$ mm. Bigger vertical offset increases the size of excluded functional regions which increases the final mass. Changing lateral offset produced a smaller effect as the excluded geometry does not change as drastically. However, leaning towards negative values generally produced slightly better results as can be seen in Figure 18. The best geometry was generated at $Z = 40$ mm and $x = -10$ mm with a final mass of 0.552 kg, while the worst was at $Z = 60$ mm and $x = 5$ mm with a mass of 0.805 kg. Compared to the configuration $Z = 40$ mm, $x = 0$ mm, the best result reduced mass from 0.580 kg to 0.552 kg, which is a 4.8% improvement.

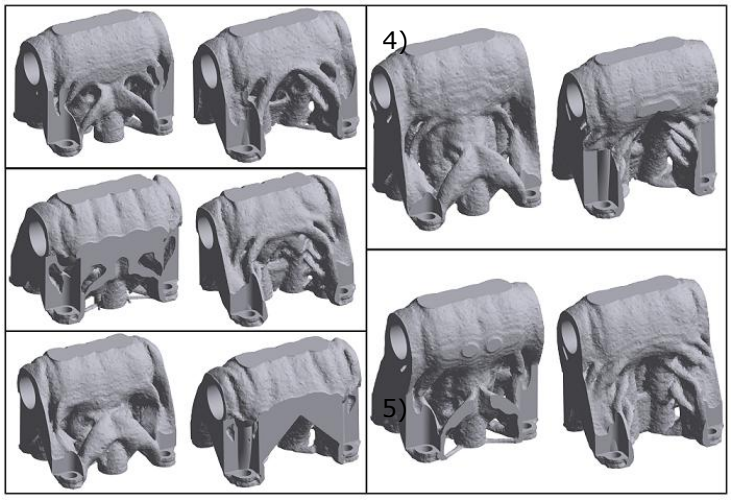

Figure 17: Final optimized geometries for spool bore position configurations: 1) $Z = 40$ mm, $x = 0$ mm, 2) $Z = 40$ mm, $x = -10$ mm, 3) $Z = 40$ mm, $x = 10$ mm, 4) $Z = 60$ mm, $x = -10$ mm and 5) $Z = 60$ mm, $x = 10$ mm.

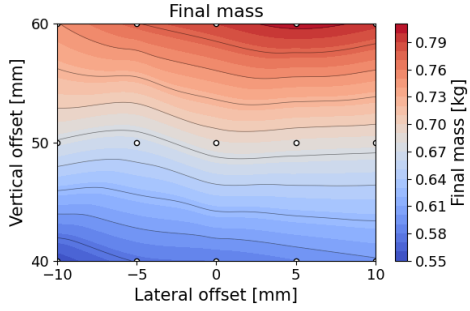

Figure 18: Calculated colourmap results of final mass obtained from TO for different lateral and vertical offsets of spool bore.

5.3 Trade-off Analysis

The trade-off analysis demonstrated that spool bore position has a clear and non-uniform influence on the structural and hydraulic performance of the valve. No configuration simultaneously minimizes mass, pressure drop, and TKE dissipation as seen in Table 1. Among the investigated cases, the lowest mass was obtained for the configuration $Z = 40$ mm, $x = -10$ mm, with a mass of 0.552 kg, whereas the minimum pressure drop was achieved at $Z = 60$ mm, $x = 0$ mm, with a value of 14.95 MPa. The lowest TKE was found at $Z = 40$ mm, $x = 5$ mm, where it reached 95.3 m²/s². This confirms that the structural optimum and the hydraulic optimums do not coincide. Distribution of the solutions indicates that the most balanced designs are concentrated primarily at $Z = 40$ mm, while increasing the spool bore vertical offset generally leads to a substantial mass penalty. Only the case $Z = 60$ mm, $x = 0$ mm remains competitive when pressure drop performance is a priority. This compensates for its relatively high mass and elevated TKE. Overall, the results suggest that spool bore vertical offset should be kept low when mass efficiency is prioritized, whereas compromises in valve weight may be acceptable when minimizing hydraulic losses becomes the dominant design objective. Based on considered metrics, $Z = 40$ mm and $x = 5$ mm represents the most balanced configuration. It has the best result for TKE dissipation, second best result for pressure drop and final mass close to the best results as can be seen in Figure 19.

Configuration number	Vertical offset Z [mm]	Lateral offset x [mm]	Pressure drop [MPa]	TKE dissipation [m²/s²]	Final mass [kg]
1	40	-10	15.50	120.2	0.552
2	40	-5	15.23	137.2	0.576
3	40	0	15.32	115.4	0.580
4	40	5	15.15	95.3	0.589
5	40	10	15.62	180.6	0.598
6	50	-10	15.51	150.3	0.673
7	50	-5	15.54	157.1	0.666
8	50	0	15.37	141.6	0.688
9	50	5	15.23	132.3	0.687
10	50	10	15.71	186.8	0.684
11	60	-10	15.58	148.5	0.749
12	60	-5	15.46	161.3	0.774
13	60	0	14.95	180.0	0.790
14	60	5	15.71	138.2	0.805
15	60	10	15.39	202.0	0.794

Table 1: CFD and TO results for all configurations.

To provide a more formal interpretation of the trade-offs, the evaluated configurations were analysed using Pareto dominance. Final mass, pressure drop, and TKE were treated as minimization objectives. A configuration was considered dominated if another configuration achieved equal or lower values in all three criteria and a strictly lower value in at least one of the evaluated metrics. Configurations 1, 2, 3, 4, and 13 were identified as not dominated. This confirms that no single spool bore position simultaneously minimizes all performance criteria. Therefore, the final design selection depends on whether mass reduction, pressure drop or TKE is prioritized.

The same assumptions and boundary conditions were used for all configurations to enable a consistent relative comparison of spool bore positions. Consequently, the reported trends should be interpreted within the selected operating conditions and design space. Changes in flow rate, spool opening, fluid, turbulence model, loading conditions, supports or TO parameters may affect the absolute values of the evaluated metrics and could influence the ranking of configurations and the

observed trade-off patterns. A full sensitivity analysis was outside the scope of this study, but it represents an important step for future validation.

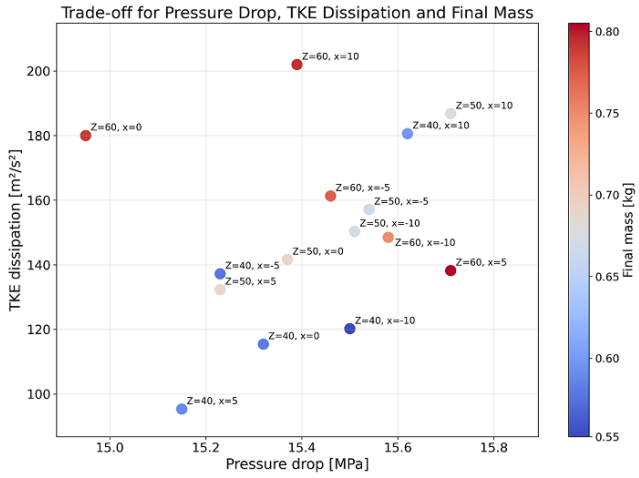

Figure 19: Results for mass, pressure drop and TKE depending on the spool bore position

6 CONCLUSIONS AND FUTURE WORK

This study demonstrated that spool bore position is an important design variable in AM hydraulic valves, as it affects both the material distribution for desired structural response of the valve body and its hydraulic performance. By evaluating CFD and TO results within a parametric study of 15 spool bore positions, it was shown that spool bore vertical offset has a stronger influence on final mass, whereas lateral offset has a greater influence on pressure drop and turbulence-related flow behaviour. The lowest final mass was obtained at $Z = 40$ mm and $x = -10$ mm which was a 4.8% improvement. The minimum pressure drop was achieved at $Z = 60$ mm and $x = 0$ mm, while the minimum TKE dissipation was observed at $Z = 40$ mm and $x = 5$ mm, meaning 1.8% and 17.4 % improvement respectively. Overall, the results confirm the problem of conflicting objectives and show that spool bore positioning should be treated as an active design parameter in the early design stage when developing lightweight and hydraulically efficient valves.

From a methodological perspective, the proposed workflow provides a structured approach for integrating multiple simulation domains within a unified design process. It enables early identification of conflicting objectives and supports informed decision making during early development. The proposed workflow is not limited to the investigated valve type and can be extended to other hydraulic systems, especially in the context of AM.

Although the authors are aware of key AM constraints such as surface roughness, overhanging geometries, depowdering, and tolerances, this study primarily focuses on the development of the workflow. Since the appropriate elimination of overhanging geometries is the most influential AM constraint in the design phase, it was explicitly considered during the TO process, thereby eliminating the need for support structures. As tight tolerances and proper fitting with the spool must be achieved, postprocessing in the form of machining is required; however, this aspect is beyond the scope of the present study.

A natural next step of the present work is prototype validation of selected configurations through manufacturing and experimental testing. Before manufacturing, TO results must be converted into smooth CAD geometry. This requires extraction of the optimized material boundary, smoothing, removal of numerical artefacts and geometric reconstruction. The reconstructed CAD model should then be verified structurally and hydraulically before AM preparation and printing. The resulting

prototypes could then be experimentally tested to evaluate hydraulic quantities such as pressure drop and leakage under representative operating conditions, followed by a comparison between CFD predictions and measured results.

ACKNOWLEDGEMENT

This research has been financially supported by the Slovenian Research and Innovation Agency (ARIS) as part of the research and infrastructure programmes No. P2-0231 and P2-0425, "Decentralized solutions for the digitalization of industry and smart cities and communities" and Young Researcher Programme.

Jan Bartolj, https://orcid.org/0009-0005-9122-6404
Aljaž Žafran, https://orcid.org/0009-0001-6974-4310
Nikola Vukašinović, https://orcid.org/0000-0003-4708-0469
Franc Majdič, https://orcid.org/0000-0002-6053-9206

REFERENCES

[1] Arena, M.; Ambrogiani, P.; Raiola, V.; Bocchetto, F.; Tirelli, T.; Castaldo, M.: Design and Qualification of an Additively Manufactured Manifold for Aircraft Landing Gears Applications, Aerospace, 10(1), 2023, 69. https://doi.org/10.3390/aerospace10010069
[2] Bartolj, J.: 3D printing for hydraulic components, International Conference Fluid Power 2023, University of Maribor Press, Maribor, 2023. https://doi.org/10.18690/um.fs.5.2023.15
[3] Bartolj, J.: Additive manufacturing in fluid power applications, Svet strojništva, 2025. http://doi.org/10.62020/svet.str.as2025005
[4] Bartolj, J.; Trajkovski, A.; Hočevar, M.; Schmitz, K.; Majdič, F.: SLM 3D printed proportional directional water hydraulic valve, tested with optimized mounting plate, in: The 19th Scandinavian International Conference on Fluid Power, River Publishers, Gistrup, 2025. http://doi.org/10.13052/rp-9788743808251A02
[5] Bendsøe, M. P.; Sigmund, O.: Topology Optimization: Theory, Methods, and Applications, Springer, Berlin, 2004. http://doi.org/10.1007/978-3-662-05086-6
[6] Beutler, P.; Berger, M.; Ferchow, J.; Meboldt, M.: Enhanced Design Automation for Hydraulic Manifolds Produced Using Additive Manufacturing, Procedia CIRP, 128, 2024, 162–167. https://doi.org/10.1016/j.procir.2024.06.017
[7] Biedermann, M.; Beutler, P.; Meboldt, M.: Automated design of additive manufactured flow components with consideration of overhang constraint, Additive Manufacturing, 49, 2021, 102119. https://doi.org/10.1016/j.addma.2021.102119
[8] CETOP – European Fluid Power Committee: CETOP RP 121H — Mounting surfaces for directional control valves, size 10 (NG10), CETOP, Brussels, 2013.
[9] DebRoy, T.; Wei, H. L.; Zuback, J. S.; Mukherjee, T.; Elmer, J. W.; Milewski, J. O.; Beese, A. M.; Wilson-Heid, A.; De, A.; Zhang, W.: Additive manufacturing of metallic components – Process, structure and properties, Progress in Materials Science, 92, 2018, 112–224. https://doi.org/10.1016/j.pmatsci.2017.10.001
[10] Diegel, O.; Schutte, J.; Ferreira, A.; Chan, Y. L.: Design for additive manufacturing process for a lightweight hydraulic manifold, Additive Manufacturing, 36, 2020, 101446. https://doi.org/10.1016/j.addma.2020.101446
[11] Gibson, I.; Rosen, D.; Stucker, B.; Khorasani, M.: Additive Manufacturing Technologies, 3rd ed., Springer, Cham, 2021. https://doi.org/10.1007/978-3-030-56127-7
[12] Herzog, D.; Seyda, V.; Wycisk, E.; Emmelmann, C.: Additive manufacturing of metals, Additive Manufacturing, 2016. https://doi.org/10.1016/j.actamat.2016.07.019

[13] Hofmann, U.; Beutler, P.; Haselbach, O.; Meboldt, M.: Automated layout optimization for hybrid additively manufactured hydraulic manifolds, Rapid Prototyping Journal, 31(11), 2025, 345–363. https://doi.org/10.1108/RPJ-04-2025-0135
[14] Hofmann, U.; Fankhauser, M.; Willen, S.; Inniger, D.; Klahn, C.; Löffel, K.; Meboldt, M.: Design of an additively manufactured hydraulic directional spool valve: an industrial case study, Virtual and Physical Prototyping, 18(1), 2023, e2129699. https://doi.org/10.1080/17452759.2022.2129699
[15] International Organization for Standardization: ISO 4401:2019 Hydraulic fluid power — Four-port directional control valves — Mounting surfaces, ISO, Geneva, 2019.
[16] Lee, T.-U.; Xie, Y. M.: Simultaneously optimizing supports and topology in structural design, Finite Elements in Analysis and Design, 197, 2021, 103633. http://doi.org/10.1016/j.finel.2021.103633
[17] Liu, J.; Ma, Y.: A Survey of Manufacturing-Oriented Topology Optimization Methods, Advances in Engineering Software, 100, 2016, 161–175. https://doi.org/10.1016/j.advengsoft.2016.07.017
[18] Ma, M.; Zhang, H.; Zhang, J.; Wang, C.: Automatic design of hydraulic manifold block based on 3D printing, Journal of Physics: Conference Series, 1087(4), 2018, 042087. https://doi.org/10.1088/1742-6596/1087/4/042056
[19] Maruyama, S.; Yamasaki, S.; Yaji, K.; Fujita, K.: Topology optimization incorporating external variables with metamodeling, Structural and Multidisciplinary Optimization, 62, 2020, 2455–2466. http://doi.org/10.1007/s00158-020-02616-1
[20] Matthiesen, G.; Merget, D.; Rückert, M.; Schmitz, K.; Schleifenbaum, J. H.: Additive manufacturing processes in fluid power – Properties and opportunities demonstrated at a flow-optimized fitting, in: Proceedings of 2018 International Conference on Hydraulics and Pneumatics – HERVEX, Băile Govora, Romania, 2018, 223–230.
[21] Rong, J.-Q.; Rong, Y.; Liu, H.; Feng, X.-Q.; Zhao, Z.-L.: Structural topology optimization method with adaptive support design, Advances in Engineering Software, 201, 2025, 103830. http://doi.org/10.1016/j.advengsoft.2024.103830
[22] Rolinck, N.; Schmitt, M.; Schneck, M.; Schlick, G.; Schilp, J.: Development Workflow for Manifolds and Fluid Components Based on Laser Powder Bed Fusion, Applied Sciences, 11(16), 2021, 7335. https://doi.org/10.3390/app11167335
[23] Schumacher, C.: Design for additive manufacturing of fluid components, RWTH Aachen University, Aachen, 2018.
[24] Semini, C.; Goldsmith, J.; Manfredi, D.; Calignano, F.; Ambrosio, E. P.; Pakkanen, J.; Caldwell, D. G.: Additive manufacturing for agile legged robots with hydraulic actuation, in: Proceedings of the 2015 International Conference on Advanced Robotics (ICAR), Istanbul, Turkey, 2015, 123–129. https://doi.org/10.1109/ICAR.2015.7251444
[25] Sigmund, O.; Maute, K.: Topology optimization approaches: A comparative review, Structural and Multidisciplinary Optimization, 48(6), 2013, 1031–1055. http://doi.org/10.1007/s00158-013-0978-6
[26] Tappeiner, Z.; Donners, M.; Schmid, M.; Schmitz, K.: Additive manufacturing of hydraulic components – pressure loss comparison of different self-supporting channel geometries, 14th International Fluid Power Conference, Dresden, River Publishers, 2024, 267–280. http://doi.org/10.13052/rp-9788770042222C20
[27] Thompson, M.; Moroni, G.; Vaneker, T.; Fadel, G.; Campbell, R.; Gibson, I.; Bernard, A.; Schulz, J.; Graf, P.; Ahuja, B.; Martina, F.: Design for additive manufacturing: trends, opportunities, considerations, Virtual and Physical Prototyping, 2024. https://doi.org/10.1016/j.cirp.2016.05.004
[28] Wohlers, T.; et al.: Wohlers Report 2024: Additive manufacturing and 3D printing state of the industry, Wohlers Associates powered by ASTM International, Fort Collins, 2024
[29] Xie, G.; Dong, Y.; Zhou, J.; Sheng, Z.: Topology optimization design of hydraulic valve blocks for additive manufacturing, Proceedings of the Institution of Mechanical Engineers, Part C:

Journal of Mechanical Engineering Science, 234(10), 2020, 1899–1912. https://doi.org/10.1177/0954406220902166
[30] Zheng, B.; Chang, C.-j.; Gea, H. C.: Topology optimization with design-dependent pressure loading, Structural and Multidisciplinary Optimization, 38, 2009, 535–543. http://doi.org/10.1007/s00158-008-0317-5